Edinburgh Research Explorer

Human astrocytic grid networks patterned in parylene-C inlayed SiO2 trenches

Corresponding Author: Dr charles unsworth,

Corresponding Author's Institution: University of Auckland

First Author: Melissa D Jordan, PhD

Order of Authors: Melissa D Jordan, PhD; Brad J Raos, BSc; Andrew S Bunting, PhD; Alan F Murray, PhD; Euan S Graham, PhD; charles unsworth

Abstract: Recent literature suggests that glia, and in particular astrocytes, should be studied as organised
networks which communicate through gap junctions. Astrocytes, however, adhere to most surfaces
and are highly mobile cells. In order to study, such organised networks effectively in vitro it is
necessary to influence them to pattern to certain substrates whilst being repelled from others and to
immobilise the astrocytes sufficiently such that they do not continue to migrate further whilst under
study.
In this article, we demonstrate for the first time how it is possible to facilitate the study of organised
patterned human astrocytic networks using hNT astrocytes in a SiO2 trench grid network that is
inlayed with the biocompatible material, parylene-C. We demonstrate how the immobilisation of
astrocytes lies in the depth of the SiO2 trench, determining an optimum trench depth and that the
optimum patterning of astrocytes is a consequence of the parylene-C inlay and the grid node spacing.
We demonstrate high fidelity of the astrocytic networks and demonstrate that functionality of the hNT
astrocytes through ATP evoked calcium signalling is also dependent on the grid node spacing.
Finally, we demonstrate that the location of the nuclei on the grid nodes is also a function of the grid
node spacing.
The significance of this work, is to describe a suitable platform to facilitate the study of hNT
astrocytes from the single cell level to the network level to improve knowledge and understanding of

how communication links to spatial organisation at these higher order scales and trigger in vitro
research further in this area with clinical applications in the area of epilepsy, stroke and focal cerebral
ischemia.

Human Astrocytic Grid Networks
Patterned in Parylene-C inlayed SiO$_2$ Trenches

M.D. Jordan[1], B.J. Raos[1], A.S. Bunting[3], A.F. Murray[3], E.S. Graham[2], C.P. Unsworth[1]

[1] Department of Engineering Science, The University of Auckland, Private Bag 92019, Auckland 1142, New Zealand.

[2] Department of Pharmacology & Centre for Brain Research, Faculty of Medical and Health Sciences, The University of Auckland, Private Bag 92019, Auckland 1142, New Zealand.

[3] Institute for Integrated Micro & Nano Systems and The Scottish Microelectronics Centre, School of Engineering & Electronics, The University of Edinburgh, EH9 3JL, UK.

Abstract

Recent literature suggests that glia, and in particular astrocytes, should be studied as organised networks which communicate through gap junctions. Astrocytes, however, adhere to most surfaces and are highly mobile cells. In order to study, such organised networks effectively *in vitro* it is necessary to influence them to pattern to certain substrates whilst being repelled from others and to immobilise the astrocytes sufficiently such that they do not continue to migrate further whilst under study.

In this article, we demonstrate for the first time how it is possible to facilitate the study of organised patterned human astrocytic networks using hNT astrocytes in a SiO$_2$ trench grid network that is inlayed with the biocompatible material, parylene-C. We demonstrate how the immobilisation of astrocytes lies in the depth of the SiO$_2$ trench, determining an optimum trench depth and that the optimum patterning of astrocytes is a consequence of the parylene-C inlay and the grid node spacing. We demonstrate high fidelity of the astrocytic networks and demonstrate that functionality of the hNT astrocytes through ATP evoked calcium signalling is also dependent on the grid node spacing. Finally, we demonstrate that the location of the nuclei on the grid nodes is also a function of the grid node spacing.

The significance of this work, is to describe a suitable platform to facilitate the study of hNT astrocytes from the single cell level to the network level to improve knowledge and understanding of how communication links to spatial organisation at these higher order scales and trigger *in vitro* research further in this area with clinical applications in the area of epilepsy, stroke and focal cerebral ischemia.

1. Introduction

1.1 The Astrocyte & Astrocytic Networks

The human brain contains approximately 86 billion neurons [1] with traditional network models of the brain being based around the neuron and neural network behaviour [2]. However, the brain also

consists of a similar number of non-neuronal cells [1] and in the last 10 years, research has revealed that the glial cell, in particular the astrocyte [3], has more functionality than the simple perfunctory support role to the neuron than was traditionally believed [4-6]. This functionality has spanned immunological signalling [7-9], endocannabinoid synthesis [10], a source of cytokines and chemokines [11] with the most unanticipated functionality being discovered in the direct modulation of the synapses of neurons through gap junctions of astrocytes [12-14] which has attracted wide attention and study. Furthermore, it has been reported how the dysfunction of astrocytes and their intimate relationship with neurons can lead to neurological disorders [15-17].

In this article, we employ the human hNT astrocyte derived from the human teratocarcinoma cell line (NTera2/D1) [18]. hNTs have been used for cell transplantation in stroke therapy [19], express ubiquitous neuronal/astrocytic markers [20] and have been directly compared to the properties of primary human cells and demonstrated to be a valid alternative to human primary astrocytes [21]. In addition, hNTs raise no ethical concerns as the derived astrocytes and neurons come from an immortalised stem cell line [20]. Thus, hNTs provide a simple and convenient human model for pursuing the aim of this work.

Recent contemporary research has posed a new challenge for scientists to now investigate the 'Astrocytic Network', as a parallel to neural networks, in order to understand how this form of network communicates through gap junctions and interacts with neurons at larger network scales [22]. *In vitro* research into this type of network could hold clues into the development of novel strategies to target subsets of astrocytes for the treatment of neurological conditions such as epilepsy, stroke and focal cerebral ischemia [15-17].

1.2 Cell Patterning & Biomaterial Parylene-C

Since astrocytes grow in a complicated Daedalean fashion, *in vitro* (shown in Fig.1), it is difficult to map the connective architecture that links single astrocyte cells together and hence determine how this affects the downstream large scale behaviour of a network.
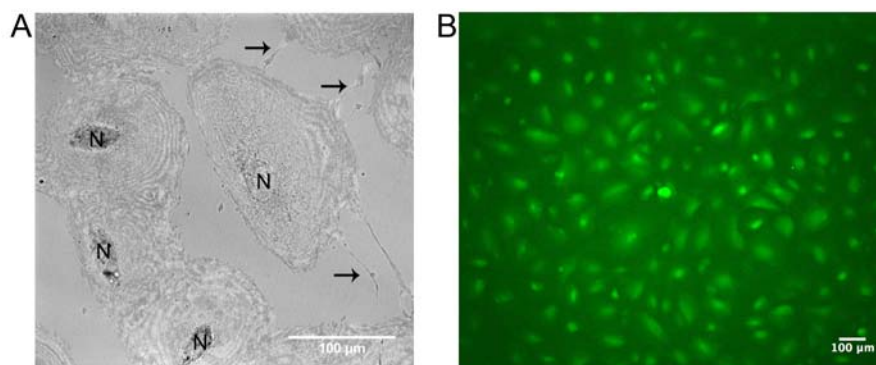
Fig. 1. Typical hNT astrocytic networks *in vitro*. (A) Brightfield reflection image of multiple astrocytes forming connections to each other. Nuclei are indicated, N, and arrows point to astrocytic processes. (B) A fluorescence image demonstrating the complex nature of the astrocytic network at high confluence.

Thus, over the last 45 years, engineering and biology have attempted to deconstruct these component cells and re-organise them in simpler ways to allow for study. This has resulted in the development of a contemporary field of study concerned with the controlling and arrangement of cells, known as 'Cell Patterning' [23]. Cell patterning, originated from metal deposition patterning in the late 1960's by

Carter [24], which broadened considerably in subsequent years to encompass photolithography, pioneered by Kleinfeld [25], and soft lithography to produce micro-contact printing introduced by Whitesides [26] and more recently inkjet printing of cells, introduced by Klebe [27] which will most likely supersede these methods when higher patterning resolutions can be obtained. Variants of these patterning methods have since been extended to encompass multiple cell types [23], co-cultures [28] and combined with Multi-Electrode Arrays (MEAs) for electrical cell recording [2].

Parylene-C [29] is a member of the parylene family which falls into the class of polymerised para-xylelene polymers. The chemical makeup of Parylene-C consists of polymerised para-xylelene where one aromatic hydrogen on each of the phenyl groups has been substituted with chlorine. Parylene-C hosts a broad span of useful properties, such as a low gas and water permeability, good electrical insulation and acid resistance. In addition, it can be fast deposited via chemical vapor deposition (CVD), providing a uniform conformal surface that is pinhole free making it attractive for semi-conductor manufacture.

In addition, parylene-C is also a bio-friendly material [29] and has previously been used in stencils, 3D cages for cell guidance and hydrophobic/hydrophilic bases that could be modified electrically [30-33]. In 2009, Delivopoulos introduced a high fidelity technique for patterning rat primary neurons on parylene-C, based around Selective Molecular Assembly Patterning (SMAP) [34] demonstrating that if parylene-C was initially treated with piranha acid that it would allow for the effective absorption of equine serum [35]. Delivopoulos also demonstrated later how photo-oxidation can disrupt parylene-C patterning [36]. This was extended by Unsworth who patterned rat primaries to the single cell level on ultra-thin parylene-C [37]. Unsworth also demonstrated how parylene-C could be used to pattern the hNT neuron [38] and hNT astrocyte [39] derived from the human teratocarcinoma cell line to the single cell level and Raos demonstrated how infra-red, laser ablated parylene-C [40] could be used for rapid pattern prototyping using hNT astrocytes. This work has been further extended by Hughes [41] who demonstrated how to modulate the pattern adhesion properties for HEK293 cells on parylene-C. Most recently, Delivopoulos demonstrated how the ratio of the fibronectin and albumin on the parylene-C and SiO_2 surfaces played an important role in cell patterning [42], Trantidou [43] demonstrated parylene-C could be laser modified for the micropatterning of rat ventricular fibroblasts and neonatal myocytes and Golda-Cepa [44] demonstrated how parylene-C when functionalized with oxygen plasma could promote cell growth for the MG-63 human osteosarcoma cell line.

In the field of cell patterning, construction of organised networks is typically performed using simple linear links in order to easily map the flow of information from the single cell level to large network scales. Hence, grid patterns are one of the simplest linear forms commonly used in cell patterning. Whilst many groups have demonstrated grid patterning of neurons in the absence of astrocytes and co-cultures of neuronal and glial cells grid arrangements [2], the patterning of grid networks of astrocytes has not been performed. In 2010, Unsworth piloted rough patterning of astrocyte networks of rat primaries, where the somas became attached to isolated nodes of parylene-C [45] but without control of the cytoplasm. In this article, our motivation is to provide a chip platform that can be readily used to accurately pattern astrocytic networks using a close human astrocyte model that tackles the issues of the highly adherent and mobile astrocyte.

2. Materials & Methods

2.1. Micro-fabrication of parylene-C inlayed SiO_2 trenches

3

The protocol used for the micro-fabrication of the parylene-C inlayed SiO_2 trenches is given below:

1. 3" diameter <100> N(Phos) 1-10 Ω.cm single side polished silicon wafers were treated with an oxygen plasma for 30 min in and Electrotech PF-xxx barrel asher to dehydrate the surface.
2. Using an SVG 8600 track system, the surface of the wafers were primed with HMDS under vacuum at a temperature of 100 °C for 30 s, spin coated with Shipley SPR350 positive working photoresist at 4000 rpm for 30 s and soft baked at a temperature of 90 °C for 60 s to give a final film thickness of 1.3 μm.
3. The trench pattern, shown in Fig. 2, was transferred from a 4" anti-reflection chrome on soda lime photomask (Compugraphics International Ltd) using a Karl Suss MA8 mask aligner with an exposure time of 6.0 s at a lamp intensity in the plane of the wafer of 4.0 mW/cm^2.
4. The pattern was developed using Shipley Microposit MF26A TMAH-based developed for 60 s at room temperature before rising in de-ionised water (18 M Ω.cm) and spinning dry, again using the SVG 8600 track system.
5. The trenches were etched into the surface of the silicon wafer using an a Bosch-style process in an STS ICP etch system (passivate: 130 sccm C_4F_8, 10 mT, 600 W coil power for 8 s, etch: 130 sccm SF_6, 13 sccm O_2, 10mT, 600 W coil power, 12 W electrode power for 12 s giving an average etch depth of 0.7 μm per cycle). Etch depths of 4 μm, 10 μm and 30 μm were produced on 3 separate wafers. Each wafer, Fig. 2, had 8 small grids with node spacing of 100 μm, 3 medium grids with node spacing 250 μm and 2 large grids with node spacing 500 μm. Each grid consisted of 10x10=100 nodes. The diameter of the trench nodes for all grids was 24 μm with the width of the trench tracks connecting the nodes being 14 μm.
6. After etching, the remaining photoresist mask thickness was measured using the Nanometrics Nanospec 3000 reflectometery system with the total trench height (remaining photoresist plus etch depth into the silicon wafer) being determined with a Veeco Instruments Dektak 8 surface profilometer. The actual etch depth into the silicon could therefore be calculated without having to remove the photoresist mask.
7. Once the correct etch depth had been obtained, the photoresist mask was removed in the Electrotech 508 barrel asher (32 sccm O_2, 700 mT, 350 W) using an etch time of 60 min.
8. The silicon wafers were loaded into a quartz boat then oxidised in an atmospheric furnace at a temperature of 1100 °C with gas flows of 1.88 SLM H_2 and 1.25 SLM of O_2 for 70 min, producing a 300 nm thick silicon dioxide layer. The thickness of the oxide layer was verified using the Nanometrics Nanospec 3000.
9. A 100 nm thick conformal coating of Parylene-C was deposited onto the wafer surface using a 67 mg charge of the monomer in a Speciality Coating Systems Lab Coater. The thickness of the Parylene film was verified by measuring the thickness of the film deposited on a small silicon witness piece, coated alongside the product wafers, again using the Nanometrics Nanospec 3000.
10. The wafers were again coated with photoresist, aligned, exposed using a second chrome mask and developed as per steps 2-4.
11. A JLS RIE 80 reactive ion etch system was used to etch away the Parylene not protected by photoresist using 50 sccm O_2 at 50 mTorr pressure and 150 W power for 2 min. The diameter of the parylene trench nodes within the grids was 20 μm with the width of the trench tracks connecting the nodes being 10 μm as determined in [39]. The parylene dimensions were verified by measurements made on a Nanometrics Nanospec 3000.
12. A protective photoresist coating was applied to the wafer surface as per step 2.
13. The wafers were diced into chips using a Disco DAD 840 wafer saw.
14. The protective photoresist layer, plus Parylene etch mask was removed by soaking the chips in acetone before rinsing in IPA then de-ionised water and finally being blown dry using a fast stream of dry N_2.
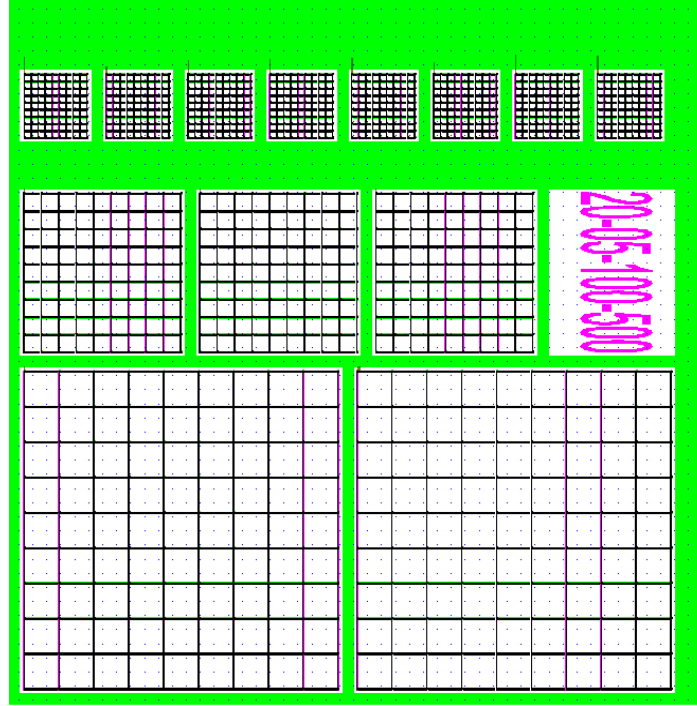
Fig. 2. Chip layout design. Chips were manufactured to the chip layout design consisting of eight small grids with node spacing of 100 μm (top row), three medium grids with node spacing of 250 μm (middle row) and two large grids with node spacing of 500 μm (bottom row). All three grid types had SiO_2 node diameters of 24 μm and trench track widths of 14 μm. The diameter of the parylene within the nodes was 20 μm with the width of the trench tracks connecting the nodes being 10 μm as determined in [39]. Separate wafers were used to realise trench depths of 4 μm, 10 μm and 30 μm.

2.2. Cleaning protocol for the parylene-C inlayed SiO_2 trench chips

The chips were removed from the wafer, briefly rinsed in acetone for 30 s and then air dried. Organic residue was then cleaned off the chips by immersion in piranha acid (30% hydrogen peroxide H_2O_2, and 98% sulphuric acid H_2SO_4, in a 5:3 ratio) for 10-15 min with frequent manual agitation. Chips were rinsed 3x in distilled water and placed onto a clean paper towel to dry. Chips were placed trench side up into a 24-well plate and sterilised for 1h at room temperature (RT) using a 1x solution of Penicillin-Streptomycin-Glutamine (PSG) (Thermofisher Scientific) in sterile Phosphate Buffered Saline (pH7.4). Following sterilisation the chips were incubated for 3 h in fetal bovine serum (FBS) (Moregate Biotech) at 37 °C and 5% CO_2. At this point the chips were ready for experimentation.

2.3. Cell culture of NTera2/D1 (NT2) cell line derived astrocytes and seeding of chips

The hNT astrocytes were differentiated over nine weeks combining protocols previously reported [38, 46]. Briefly, differentiation of precursor cells into a mixed population of hNT neurons and astrocyte precursor cells was performed over four weeks as detailed in [46]. After harvesting the neurons at week four, the astrocytes were differentiated for a further five weeks using a decreasing cocktail of mitotic inhibitors as outlined in [38]. At the conclusion of the differentiation protocol, aliquots of 2.5

5

x 10^6 astrocytic cells were cryopreserved in medium consisting 50% DMEM F12, 45% FBS (Morgate Biotech) and 5% DMSO and thawed as needed for experiments.

Astrocytes were cultured in T-25 flasks (Nunc) with DMEM F12 medium supplemented with 5% FBS, 1x penicillin-streptomycin-glutamine (PSG) and 10 μM uridine mitotic inhibitor. Cells were generally used within two weeks of being thawed. Prior to experiments cells were dissociated from the flask with 0.05% Trypsin, rinsed with medium and centrifuged at 200 *g* for 5 min. Cells were initially re-suspended in 1 ml of medium, counted, and finally re-suspended in an appropriate volume of culture medium for seeding onto the trench chips. Cells were seeded at densities of 25, 50 or 100 cells per mm^2. It was found that the chips could be incubated at 37 °C and 5% CO_2 for two days for network formation to be achieved (rather than 6 days as previously reported [39]) to allow the astrocytes to settle and adhere.

2.4. Cell labelling and imaging

For cell density and patterning analysis, cells were stained live with Cell Tracker Green CMFDA Dye (Thermofisher Scientific). The dye was made to a final concentration of 1 μM in DMEM F12 medium containing 5% FBS and 1x PSG and cells were incubated with the dye solution for 1 h at 37 °C and 5% CO_2. The dye was then removed and the cells fixed with 4% paraformaldehyde (PFA) for 15 min at RT. The cells were rinsed 1x 15 min in PBS containing Hoechst 33258 (Sigma) nuclear stain at 1:6000 dilution. Finally cells were rinsed 3x in PBS before imaging.

For calcium signalling analysis, cells were loaded with Fluo-4 AM dye (Thermofisher Scientific). The dye was made to a final concentration of 2 μM in FluoroBrite DMEM containing 1% FBS and cells were incubated with the dye solution for 1 h at 37 °C and 5% CO_2. After loading, the light exposure of the cells was kept to a minimum to prevent photo-toxicity. Cells were rinsed 2x with dye free FluoroBrite and used immediately for imaging. The neurotransmitter adenosine triphosphate (ATP) is implicated in astrocytic signalling and exposure of hNT astrocytes to ATP results in robust calcium responses reported in [21, 47]. We therefore used the calcium response to ATP to examine the functionality of the patterned hNT astrocytes in terms of their ability to signal normally. During the calcium imaging experiments, cells were continuously perfused with medium at a flow rate of 1 ml per minute using a MINIPULS Evolution peristaltic pump (Gilson).

All imaging was performed on an Olympus BX53 fluorescence microscope employing cellSens Dimension software and using a 10x UMPLFLN water immersion objective. For cell density and patterning analysis the cells were visualised using a 100 W mercury light source (U-LH100HG) and for calcium signalling analysis, a standard 100 W halogen lamp was used.

2.5. Image pre-processing

All image processing was performed using standard image processing algorithms implemented as a workflow in MATLAB (2014b, The MathWorks Inc., Natick, MA) using the Image Processing Toolbox and the OME-Bioformats library. First the individual images of each sample were corrected with a flat field image, to remove vignetting, and stitched into a single mosaic covering the whole sample. The replicated trenches on each sample were then cropped and rotated into a common reference frame for further processing. A combination of filtering, thresholding and morphological image processing was used to generate masks for cellular area. Briefly the CMFDA images were run through a 5x5 Weiner filter to suppress low level noise in the images. The images were then thresholded to a level where the remaining noise began to appear as small objects with areas of only a few pixels. The thresholded masks were then morphologically opened using a 7 pixel disk structural

6

element to remove small objects that represented noise rather than cellular content. This method minimised the amount of noise that is incorporated into the thresholded mask, which would otherwise erroneously inflate the amount of cellular content and obscure the discrimination of cellular content that is on and off the trenches. A mask representing the trench and node regions was generated by manually delineating the boundaries of each grid array (Fig. 3B). Thus, the areas of cellular and nuclear content that were 'on' and 'off' the trenches could be identified automatically (Fig. 3C-D).
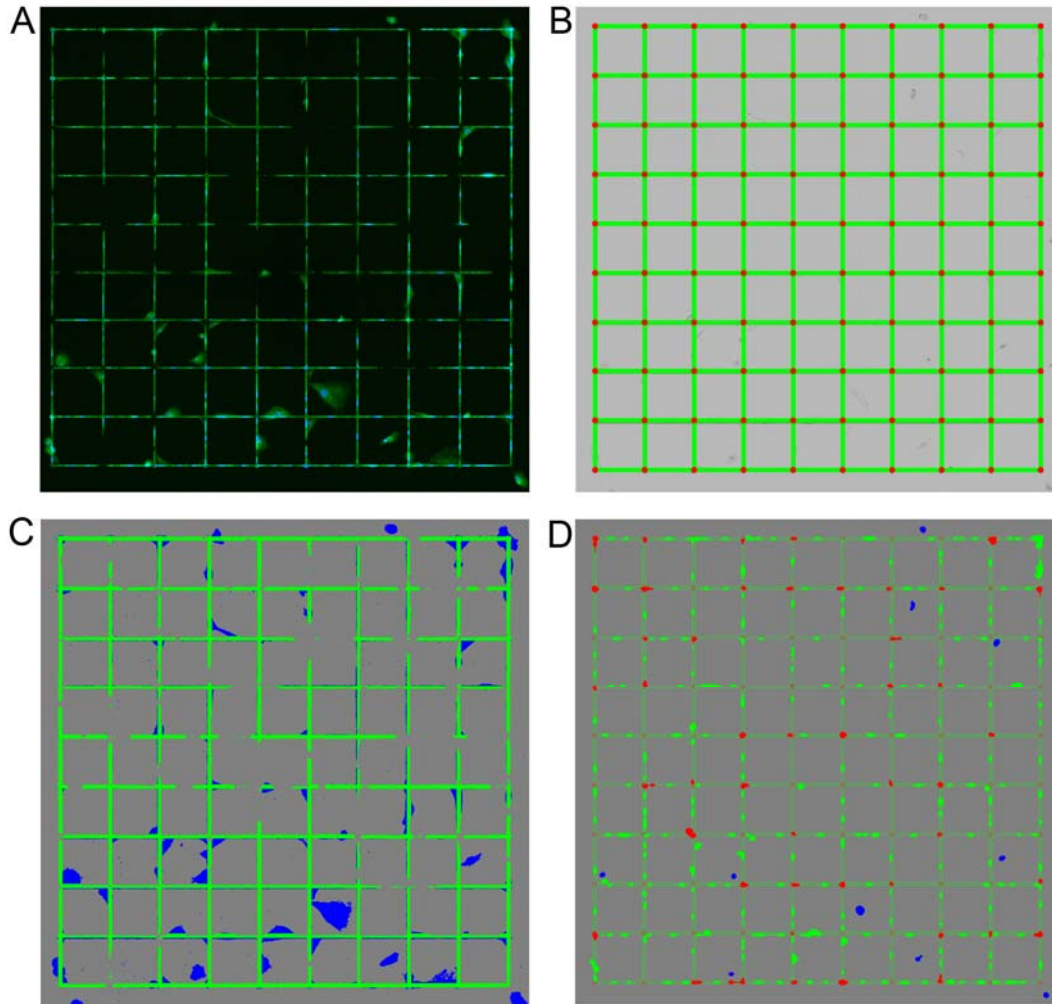

Fig. 3. (A) A typical fluorescent image of astroctyes in the grid trench network. Blue fluorescence indicates individual nuclei and green fluorescence results from CMFDA staining of the entire cell, (B) Mask used to identify cellular content on and off regions of interest (ROI) overlayed on the brightfield image. Green represents the trench ROI and red represents the node ROI, (C) Cellular content detected and quantified post image processing on and off the ROI (highlighted in pseudo colour; blue = cellular content on SiO_2, green = cellular content in trenches), (D) Nuclear content detected and quantified post image processing on and off the ROIs (highlighted in pseudo colour; blue = nuclei on SiO_2, red = nuclei within nodes, green = nuclei in trenches).

In order to measure the quality of the patterning of the astrocytic grid networks we utilised the 'parylene adhesion index' (PAI) defined in [41] as the coverage of cellular content on the parylene normalised to the total parylene area (Thus, a PAI = 1 defines a total coverage of the parylene by cells). In addition, we define an equivalent 'SiO_2 attraction index' (SAI) as the coverage of cellular

content on the SiO_2 regions within the grid network normalised to the total area of all the SiO_2 regions. (Thus, a SAI = 1 defines a total coverage of the SiO_2 by cells). This allows us to define a 'Grid Quality Index' (GQI) as, GQI = PAI – SAI. Where, $-1 \leq GQI \leq 1$. A GQI = 1 states that the astrocyte cellular content lies solely in the parylene trenches and not on adjacent SiO_2, a GQI = -1 states that the astrocyte cellular content lies solely on the adjacent SiO_2 and not in the parylene trenches and a GQI = 0 states that the astrocyte cellular content is equally distributed in both the parylene trenches and the adjacent SiO_2. Thus, a GQI =1 would be a measure of the highest fidelity of an astrocytic network.

In addition, the percentage of nuclei that were isolated at the nodes of the grids was quantified by defining a node index (NI) as, NI = number of nuclei on nodes/ total number of nuclei in trench. Thus, an NI = 1 states that 100% of the nodes were occupied by astrocytic nuclei.

3. Results

In the following sections, we quantify how trench depth and seeding density affect the patterning of the cellular content of the astrocytic networks using the GQI measure, defined in the previous section, for each of the three grid sizes. We then proceed to perform calcium functionality testing of each of the three grid sizes to identify which grids provide the best response. Finally, we quantify which of the three grid sizes provides the best isolation of nuclei at the grid nodes using the NI measure, defined in the previous section.

3.1 The effect of trench depth and cell seeding density on cell patterning

hNT astrocytes were seeded at three different cell densities, 25, 50 and 100 cells/mm^2, onto the three chip types varying in trench depth. The chip trench depths were 4 µm, 10 µm and 30 µm. The resulting combinations of cell density, trench depth and grid node spacing were imaged and analysed to determine which provided the best cell patterning. Fig. 4 highlights the patterning of the hNT astrocytes over the entire chip surface at 10× magnification for all combinations.
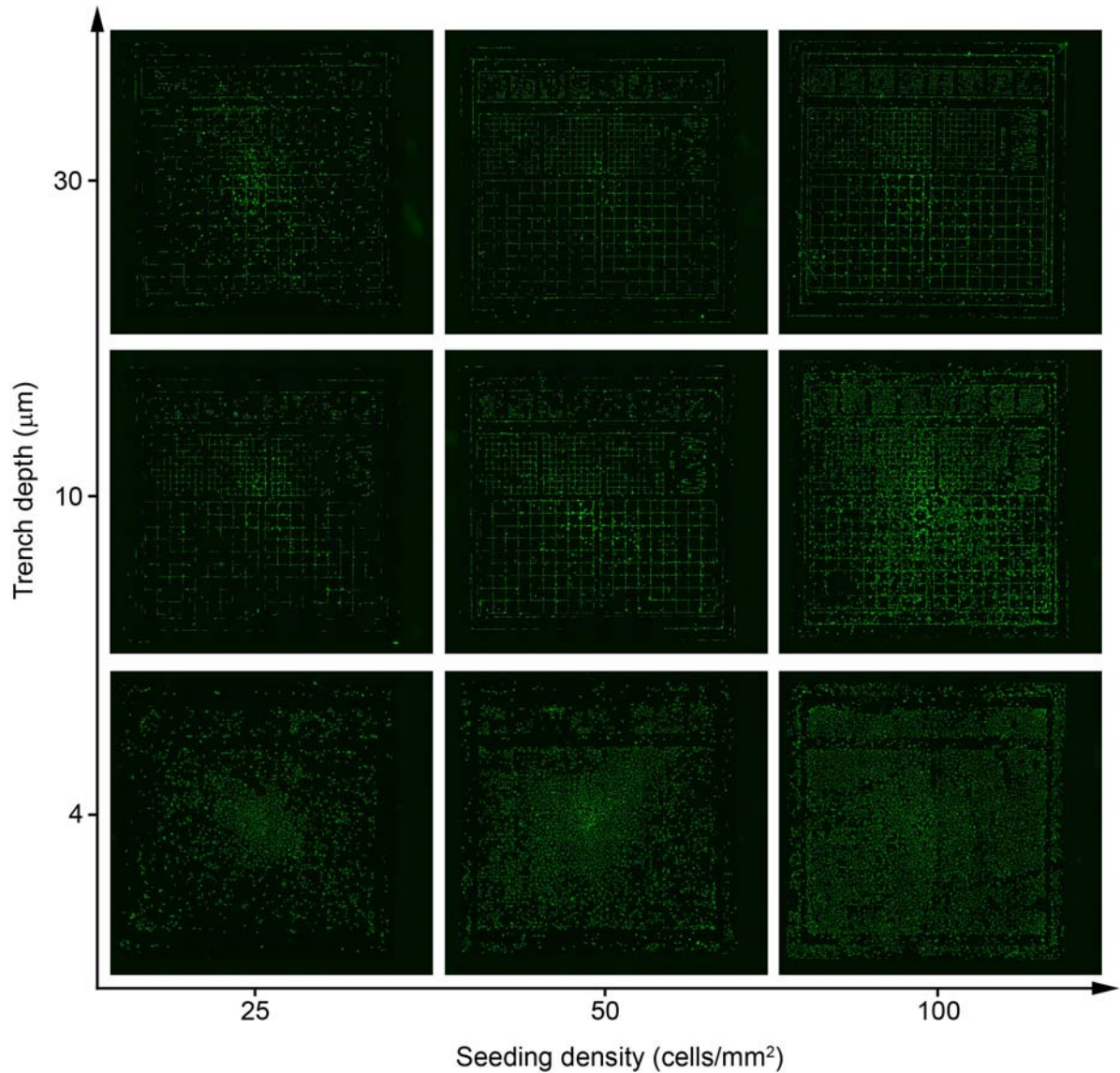
Fig. 4. hNT astrocyte grid networks produced at increasing seeding densities 25, 50 and 100 cells/mm^2 and trench depths of 4, 10 and 30 μm. Astrocytes are stained with Cell Tracker Green CMFDA live cell stain and appear green.

Initial visual observations from Fig. 4 are that no obvious patterning was observed at any cell density for the 4 μm depth trenches. At a trench depth of 10 μm, patterning was clearly observed for increasing cell density. However, at the highest cell density it was found that there tended to be more cells on the SiO_2 surface. At a trench depth of 30 μm, patterning was more clearly observed for increasing cell density and the highest cell density was preserved in the trenches rather than on the SiO_2 surface (unlike in the 10 μm case). As a point to note, for all trench depths it was observed that there seemed to be a small effect of a higher cell density in the middle of the chip, due to culturing in the round well of a 24-well plate. An additional point to note is that some cell content on the SiO_2 could also be due to there not being any available room left in the trenches for the astrocytes to migrate to.

Image analysis was performed (as described in Section 2.5), for all the individual grids on the chips and the cellular area associated within the trench and on the bare SiO_2 was calculated to determine

9

percentage coverage values for the different sized grids, trench depths and seeding densities, presented in Fig. 5.
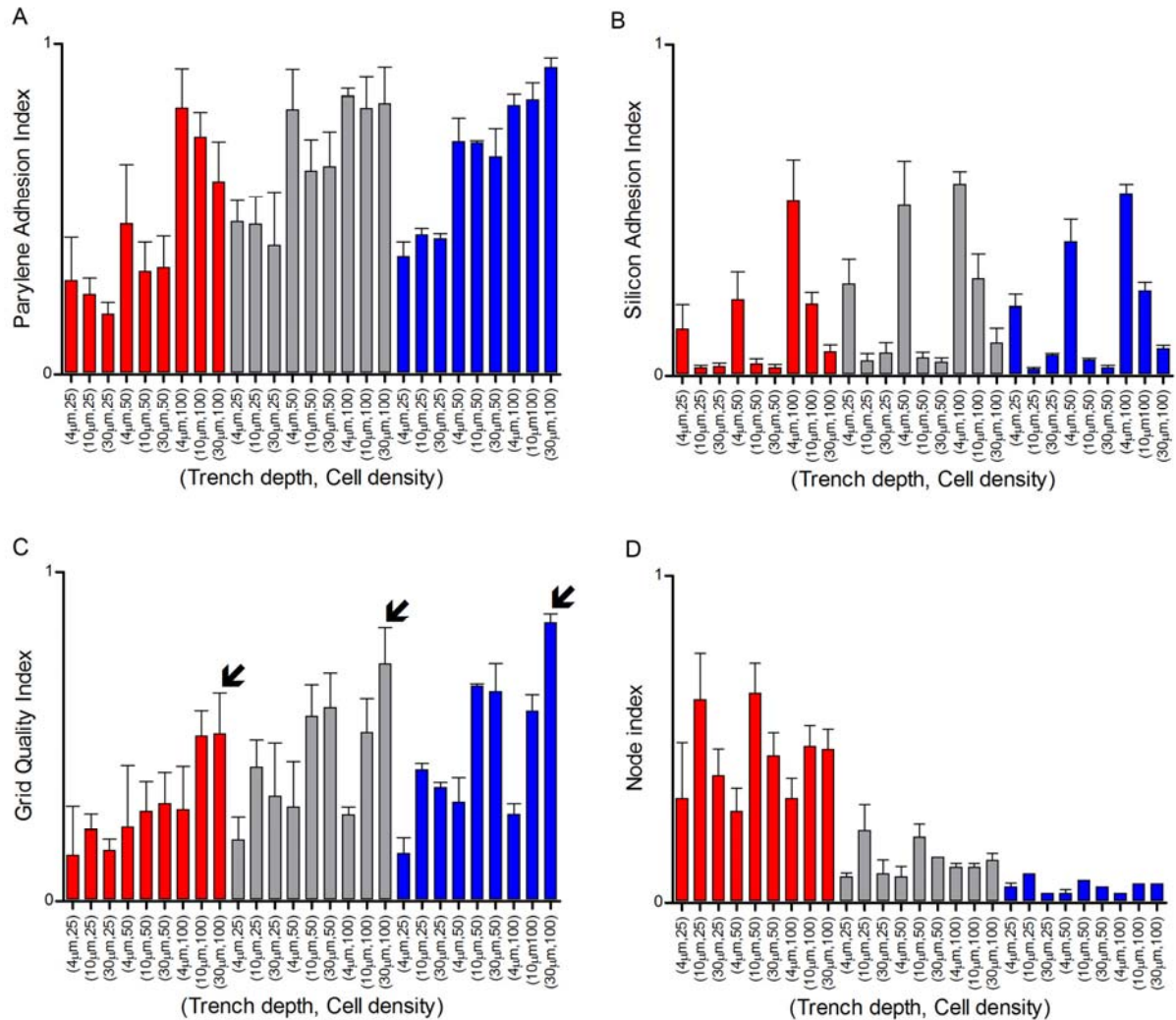

Fig. 5. Measurement of cell coverage in the grid networks for different sized grids, trench depths and seeding densities. The (A) Parylene Adhesion Index (PAI) provides a measure of the cellular coverage of the trench; (B) Silicon Adhesion Index (SAI) provides a measure of the cellular coverage of the SiO_2 area; (C) Grid Quality Index (GQI) provides a measure of the total patterning (PAI-SAI) with the best cellular coverage for each grid size highlighted by a black arrow; (D) Node Index (NI) provides a measure of the presence of cell nuclei specifically within trench nodes. Small grids with 100 µm node spacing (red), medium grids with 250 µm node spacing (grey) and large grids with 500 µm node spacing (blue)

Thus, we demonstrate, with Fig. 5, that the highest GQI was achieved for networks with increasing trench depth, cell density and node spacing. Thus, a 30 µm trench depth at 100 cells/mm^2 provided the best patterning and highest GQI firstly for the large grids with a node spacing of 500 µm, followed by

the medium grids with a node spacing of 250 μm and then by the small grids with a node spacing of 100 μm, shown in Fig. 6.
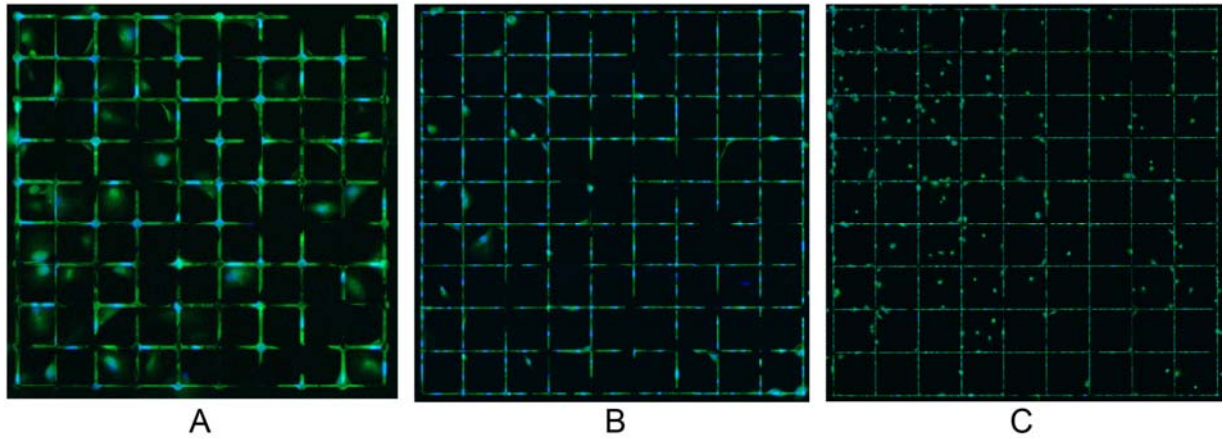

Fig. 6. Fluorescence images of astrocyte patterning for the three grid node spacings, from the 30 μm trench chip seeded at 100 cells/mm^2 that provided the best patterning and highest GQI. (A) Grid with 100 μm node spacing, (B) Grid with 250 μm node spacing and (C) Grid with 500 μm node spacing. Blue fluorescence indicates individual nuclei and green fluorescence results from CMFDA staining of the entire cell.

3.2 Measuring Functionality of hNTs Astrocytes in SiO$_2$ Trenches

The functionality of the patterned hNT astrocytes within the grid arrays was then assessed for the three grid node spacings at the 30 μm trench depth at 100 cells/mm^2. This was assessed by measuring the intracellular change in calcium in response to the introduction of ATP which has been demonstrated to trigger calcium responses effectively for hNT astrocytes in [21] as described in section 2.4.

Initially as a control, the functionality of the hNT astrocytes was determined under normal cell culture conditions in a 35 mm petri dish. The time-lapse fluorescence video of the astrocytes was imported into the freeware package ImageJ © [48] as a Z-Stack. Fluorescence measurements were made by manually creating ROIs, representing individual cells, using ImageJ's ROI management toolbox, Fig. 7A. The fluorescence values recorded represent the mean fluorescence for each ROI during every frame of the time-lapse video. The fluorescence values for each ROI were then imported into MATLAB© (2014b, The MathWorks Inc., Natick, MA) where the multi-cell time-series was plotted as a heat-map, Fig. 7B. Each horizontal line in (Fig. 7B) shows the fluorescence time-series from a single ROI and the colour represents the fluorescence intensity (with red representing the maximum calcium response for that cell) at specific points in time. The ATP was introduced at 300 seconds into the experiment and the response of the individual astrocytes can be clearly seen instantaneously at this point, (Fig. 7B) to confirm that reported in [21].
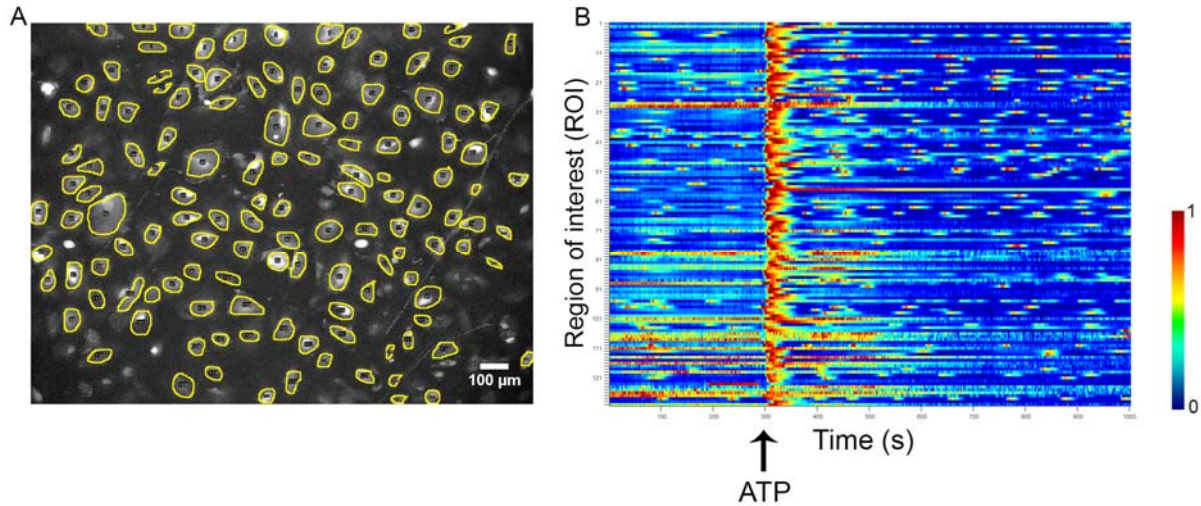
11

Fig. 7. (A) Regions of interest (ROIs) in yellow indicate individual cells selected for analysis from the fluorescence image of astrocytes in a 35 mm dish (B) A multi-cell time-series heat-map of the temporal fluorescence of all the astrocytes highlighted in (A) and triggered by introduction of ATP at 300s.

Once the functionality of the astrocyte control had been validated in a 35 mm dish [21], the functionality of the astrocytes in the parylene-C inlayed SiO_2 trenches was investigated. This was performed for the grids that provided the highest GQI, namely the 30 μm trench depth, with node spacing of 500 μm, 250 μm and 100 μm at a seeding density of 100 cells/mm^2 (as determined previously, Section 3.1, Fig. 5). Fig. 8(A-C) highlights the 30 μm trench for node spacing of 100, 250 and 500 μm at 100 cells/mm^2 respectively and Fig. 8(D-F) shows the astrocyte calcium responses occurring at 300 s to an ATP stimulus for the grids (A-C) respectively. For the 500 μm node spacing, Fig. 8C highlights that patterning was clearly obtained. However, there was hardly a discernible ATP response at 300 s in Fig. 8F as compared to the control ATP response that was clearly observed *in vitro* in Fig. 7B. It was found that for grids with a 250 μm node spacing, Fig. 8B, that patterning was clearly obtained and a very clear ATP response at 300 s in Fig. 8E that was comparable to the control ATP response observed *in vitro*, of Fig. 7B. Finally for the grids with 100 μm node spacing, Fig. 8A, patterning was clearly obtained and a very clear ATP response at 300 s in Fig. 8D that was comparable to the control ATP response observed *in vitro*, of Fig. 7B. In addition, to the ATP response observed for the 100 μm aspect ratio grids in Fig. 8D it was also evident that there was a distinct amount of calcium-dependent communication prior to the addition of ATP, which could be due to node spacing of the network and the closer proximity of the astrocytes.
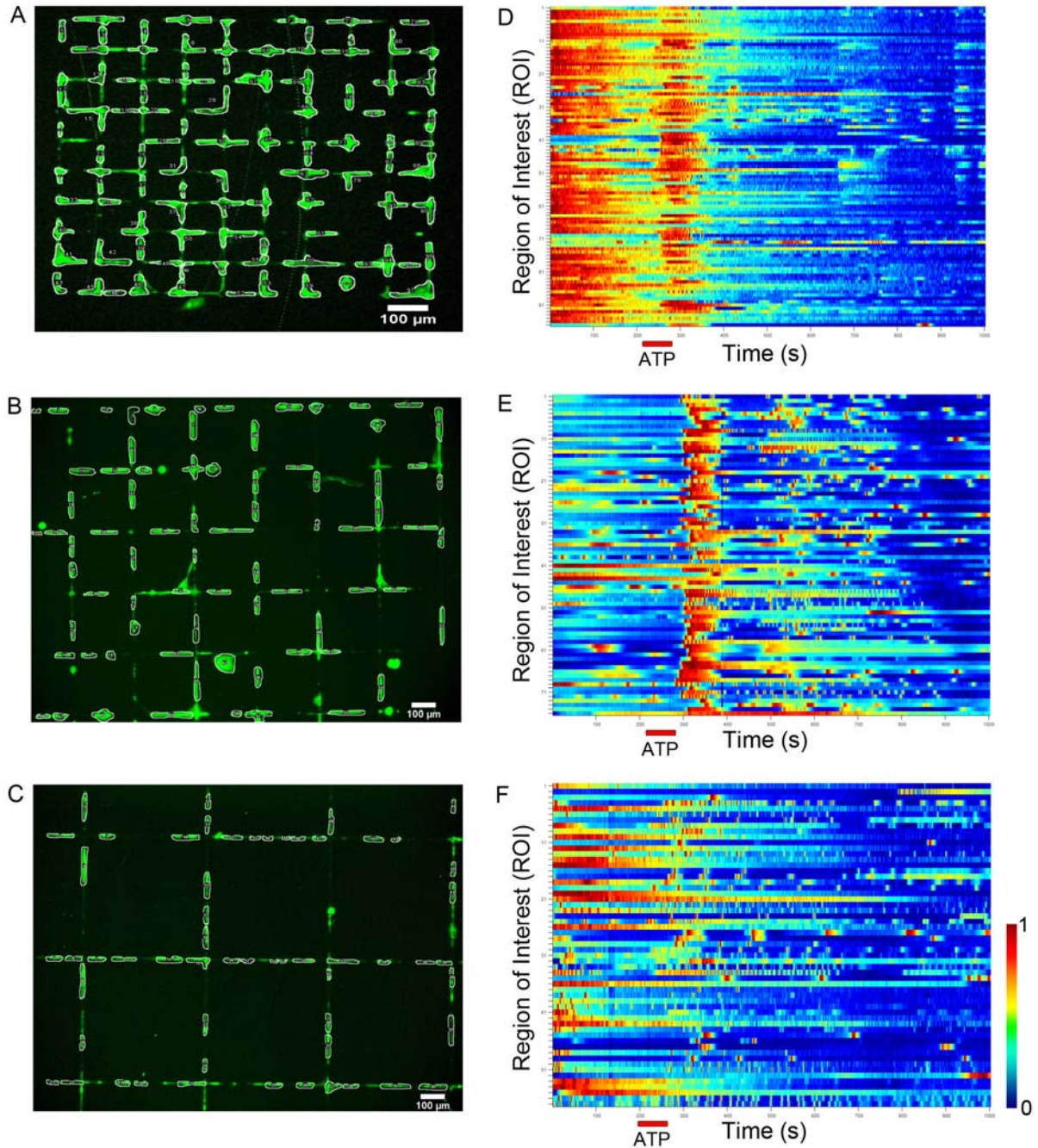
Fig. 8. Functionality testing of hNT astrocytes in grids of varying node spacing. (A-C) Fluorescent images of the 30 μm depth trench for node spacing of 100, 250 and 500 μm at 100 cells/mm^2 respectively. (D-F) Heatmaps detailing the astrocyte calcium response at approximately 300 s to ATP for the grids (A-C), respectively.

Thus, whilst the large grids (500μm node spacing) provided the highest level of patterning (highlighted by the highest GQI) they failed to provide a robust functional response. The medium grids (250μm node spacing) provided the next highest GQI and provided a good functional response as typically observed in our control response. Finally, the small grids (100μm node spacing) provided the next highest GQI and provided a good functional response as typically observed in our control response.

13

We then proceeded to assess the isolation of nuclei on the grid nodes using the NI measure, defined in section 2.5. The NI results are presented in Fig. 5(D). It can be clearly seen from Fig. 5(D) that the NI is highest for the small grids and considerably lower for medium grids and large grids. The three highest NI's were found for the 10μm trench depths for the three different cell seeding densities. This was closely followed by the 30μm trench depth at a cell seeding density of 100 cells/mm². Given that the functionality testing of the three different grid sizes yielded only the medium (250 μm node spacing) and small grids (100 μm node spacing) to be responsive to ATP stimulation and thus useful (section 3.2); and given that the best cellular coverage for the medium and small grids occurred for a trench depth of 30 μm and cell seeding density of 100 cells/mm². Then it can be seen from Fig. 5(D) that the 30 μm trench for the small grid (100 μm node spacing) provided the best overall isolation of the nuclei, cellular coverage and functionality.

4. Discussion

In this article, we have developed a suitable silicon chip platform, in the form of a parylene-C inlayed SiO₂ trench grid network, to facilitate the study of hNT astrocytes from the single cell level to the network level in order to address recent contemporary research towards the study of astrocytic networks [22]. The work details the nanofabrication and culturing protocols necessary to realise such a chip platform and reports the level of astrocytic network patterning that occurs for varying grid depths and grid node spacing. In addition, the article reports the functionality of the hNT astrocytic grid networks.

It was found that significant preferential patterning was observed as the grid depths of the SiO₂ were increased from 4 μm to 30 μm, with 30 μm trench depths providing the best level of patterning. In addition, it was found that the hNT astrocytes patterned successfully to the parylene-C inlayed SiO₂ trench grid network altering their typical flat-egg or star-like morphology to conform to the linear grid networks which was similar to the hNT behaviour reported for neurons [38] and astrocytes [39] along linear strips. It was observed that grid networks with 500 μm grid node spacing provided the highest cellular coverage, followed by the grid networks with a 250 μm grid node spacing and finally the 100 μm aspect ratio grid networks. In addition, the proportion of cellular coverage was found to be greater than 40% for all grid node spacings at the highest cell density of 100 cells per mm² which is improved upon for hNT astrocytes on simple linear strips [39]. This may suggest that the hNT astrocytes prefer architectures that permit more degrees of freedom, allowing them to communicate more diversely. We also found that the time required for culturing astrocytes into grid networks could be reduced significantly to 2 days rather than 6 days over linear strips, reported in [39] which may suggest that astrocytes mobilise quicker into trench networks rather than along linear strips.

It has been demonstrated that hNT astrocytes produce a robust calcium response to introduction of ATP [21, 47]. Calcium signalling represents a readout that can be monitored easily and continuously in real-time with minimal manipulation to the cells. In our experiments, we assessed the calcium signalling in all of the astrocytes at the single cell level, which provided a highly valuable readout over selecting representative cells. Moreover, calcium signalling in astrocytes is a physiologically very important pathway and we *hypothesised* that the functionality of astrocytic grid networks should also be evident through their calcium response to ATP. Whilst the astrocytes patterned successfully in all grid node spacings it was found that grids with 250μm and 100μm grid node spacing provided functional networks, releasing calcium throughout the whole network upon the introduction of ATP whilst the grids with 500 μm node spacing provided poor functionality. Thus, whilst hNT astrocytes

14

could be patterned in a variety of grid sizes, functional networks only occurred at medium- and small-scale networks of 100μm ≤ node spacing ≤ 250μm. We *hypothesise* that there is a close relationship between the physical size of the hNT astrocyte (which can extend from 100-200 μm in diameter) and the node spacing of the network.

Furthermore, we assessed the isolation of the astrocytic nuclei on the nodes of the grid. It was found that the isolation of nuclei was highest for the small grids of 100μm node spacing and found to be considerably lower for medium grids and large grids. From the cellular coverage results and ATP functionality testing it was then determined that the 30μm trench at 100 cells/mm^2 seeding density for the small grids (100μm node spacing) provided the best overall isolation of the nuclei, cellular coverage and functionality.

5. Conclusion

In this article, we demonstrate a chip platform, in the form of a SiO_2 trench grid network that is inlayed with parylene-C, which can facilitate the study of organised patterned hNT astrocytic networks. We demonstrate how optimum immobilisation of astrocytes lies in a SiO_2 trench depth of 30 μm. In addition, we demonstrate high fidelity of the astrocytic grid networks with optimum cellular patterning occurring when the grid node spacing was 500μm, followed by grid node spacing of 250μm and then 100μm.

In addition, we *hypothesise* that the functionality of hNT astrocytic grid networks through ATP evoked calcium signalling is consistent with the ATP evoked calcium signalling observed *in vitro*. We show that this too was dependent on the grid node spacing, being functional for 100μm and 250μm grid node spacing with the functionality being much less evident in large grid node spacing of 500μm. Hence, concluding that optimum patterning and functionality of hNT astrocytic networks prefer small and medium sized grid networks of 100μm to 250μm grid node spacing that is proportional to their diameter.

Furthermore, we demonstrated that the isolation of nuclei on the nodes of the grid networks is also a function of grid node spacing with the nuclei being found to locate much more successfully on the nodes of the small sized grids for grid node spacing 100μm. This was followed but found to be considerably less for the medium grids with grid node spacing of 250μm and less still for the large grids with grid node spacing of 500μm.

Thus, taking the three main factors of cellular coverage, Ca+ functionality and nuclei isolation on the grid nodes into consideration, it was determined that the 30μm trench at 100 cells/mm^2 seeding density for small grids networks of 100μm node spacing yielded the best overall cellular coverage, Ca$^+$ functionality and isolation of the nuclei.

The significance of the developed platform is that it will facilitate the study of hNT astrocytes from the single cell level through to network scales. This will lead to improved knowledge and understanding of how communication maps to spatial organisation for the astrocytic network. Furthermore it will enable clinical investigations into conditions such as epilepsy, stroke and focal cerebral ischemia [15-17].

References

[1] Herculano-Houzel S. The human brain in numbers: a linearly scaled-up primate brain. Front Hum Neurosci. 2009;3:31.

[2] Wheeler BC, Brewer GJ. Designing Neural Networks in Culture: Experiments are described for controlled growth, of nerve cells taken from rats, in predesigned geometrical patterns on laboratory culture dishes. Proc IEEE Inst Electr Electron Eng. 2010;98:398-406.

[3] Wang DD, Bordey A. The astrocyte odyssey. Prog Neurobiol. 2008;86:342-67.

[4] Kimelberg HK. Supportive or information-processing functions of the mature protoplasmic astrocyte in the mammalian CNS? A critical appraisal. Neuron Glia Biol. 2007;3:181-9.

[5] Kimelberg HK. The problem of astrocyte identity. Neurochem Int. 2004;45:191-202.

[6] Allen NJ, Barres BA. Neuroscience: Glia - more than just brain glue. Nature. 2009;457:675-7.

[7] Becher B, Prat A, Antel JP. Brain-immune connection: immuno-regulatory properties of CNS-resident cells. Glia. 2000;29:293-304.

[8] Chakraborty S, Kaushik DK, Gupta M, Basu A. Inflammasome signaling at the heart of central nervous system pathology. J Neurosci Res. 2010;88:1615-31.

[9] Dong Y, Benveniste EN. Immune function of astrocytes. Glia. 2001;36:180-90.

[10] Zhao L, Brinton RD. Suppression of proinflammatory cytokines interleukin-1beta and tumor necrosis factor-alpha in astrocytes by a V1 vasopressin receptor agonist: a cAMP response element-binding protein-dependent mechanism. J Neurosci. 2004;24:2226-35.

[11] Lu W, Maheshwari A, Misiuta I, Fox SE, Chen N, Zigova T, et al. Neutrophil-specific chemokines are produced by astrocytic cells but not by neuronal cells. Brain Res Dev Brain Res. 2005;155:127-34.

[12] De Pitta M, Brunel N, Volterra A. Astrocytes: Orchestrating synaptic plasticity? Neuroscience. 2015.

[13] Furshpan EJ, Potter DD. Transmission at the giant motor synapses of the crayfish. J Physiol. 1959;145:289-325.

[14] Kuffler SW, Nicholls JG, Orkand RK. Physiological properties of glial cells in the central nervous system of amphibia. J Neurophysiol. 1966;29:768-87.

[15] Halassa MM, Fellin T, Haydon PG. The tripartite synapse: roles for gliotransmission in health and disease. Trends Mol Med. 2007;13:54-63.

[16] Rogawski MA. Astrocytes get in the act in epilepsy. Nat Med. 2005;11:919-20.

[17] Seifert G, Schilling K, Steinhauser C. Astrocyte dysfunction in neurological disorders: a molecular perspective. Nat Rev Neurosci. 2006;7:194-206.

[18] Svendsen CN, ter Borg MG, Armstrong RJ, Rosser AE, Chandran S, Ostenfeld T, et al. A new method for the rapid and long term growth of human neural precursor cells. J Neurosci Methods. 1998;85:141-52.

[19] Hara K, Yasuhara T, Maki M, Matsukawa N, Masuda T, Yu SJ, et al. Neural progenitor NT2N cell lines from teratocarcinoma for transplantation therapy in stroke. Prog Neurobiol. 2008;85:318-34.

[20] Pleasure SJ, Page C, Lee VM. Pure, postmitotic, polarized human neurons derived from NTera 2 cells provide a system for expressing exogenous proteins in terminally differentiated neurons. J Neurosci. 1992;12:1802-15.

[21] Haile Y, Fu W, Shi B, Westaway D, Baker G, Jhamandas J, et al. Characterization of the NT2-derived neuronal and astrocytic cell lines as alternative in vitro models for primary human neurons and astrocytes. J Neurosci Res. 2014;92:1187-98.

16

[22] Giaume C, Koulakoff A, Roux L, Holcman D, Rouach N. Astroglial networks: a step further in neuroglial and gliovascular interactions. Nat Rev Neurosci. 2010;11:87-99.

[23] Falconnet D, Csucs G, Grandin HM, Textor M. Surface engineering approaches to micropattern surfaces for cell-based assays. Biomaterials. 2006;27:3044-63.

[24] Carter SB. Principles of cell motility: the direction of cell movement and cancer invasion. Nature. 1965;208:1183-7.

[25] Kleinfeld D, Kahler KH, Hockberger PE. Controlled Outgrowth of Dissociated Neurons on Patterned Substrates. Journal of Neuroscience. 1988;8:4098-120.

[26] Xia YN, Whitesides GM. Soft lithography. Annu Rev Mater Sci. 1998;28:153-84.

[27] Klebe RJ. Cytoscribing: a method for micropositioning cells and the construction of two- and three-dimensional synthetic tissues. Exp Cell Res. 1988;179:362-73.

[28] Goubko CA, Cao XD. Patterning multiple cell types in co-cultures: A review. Mat Sci Eng C-Mater. 2009;29:1855-68.

[29] Fortin JB, Lu TM. Chemical Vapor Deposition Polymerization: The Growth and Properties of Parylene Thin Films. 1 ed: Springer US; 2004.

[30] Chang TY, Yadav VG, De Leo S, Mohedas A, Rajalingam B, Chen CL, et al. Cell and protein compatibility of parylene-C surfaces. Langmuir. 2007;23:11718-25.

[31] Tooker A, Meng E, Erickson J, Tai YC, Pine J. Biocompatible parylene neurocages. Developing a robust method for live neural network studies. IEEE Eng Med Biol Mag. 2005;24:30-3.

[32] Wei L, Lakhtakia A, Roopnariane AP, Ritty TM. Human fibroblast attachment on fibrous parylene-C thin-film substrates. Mat Sci Eng C-Mater. 2010;30:1252-9.

[33] Wright D, Rajalingam B, Karp JM, Selvarasah S, Ling Y, Yeh J, et al. Reusable, reversibly sealable parylene membranes for cell and protein patterning. J Biomed Mater Res A. 2008;85:530-8.

[34] Michel R, Lussi JW, Csucs G, Reviakine I, Danuser G, Ketterer B, et al. Selective molecular assembly patterning: A new approach to micro- and nanochemical patterning of surfaces for biological applications. Langmuir. 2002;18:3281-7.

[35] Delivopoulos E, Murray AF, MacLeod NK, Curtis JC. Guided growth of neurons and glia using microfabricated patterns of parylene-C on a SiO2 background. Biomaterials. 2009;30:2048-58.

[36] Delivopoulos E, Murray AF, Curtis JC. Effects of parylene-C photooxidation on serum-assisted glial and neuronal patterning. J Biomed Mater Res A. 2010;94:47-58.

[37] Unsworth CP, Delivopoulos E, Gillespie T, Murray AF. Isolating single primary rat hippocampal neurons & astrocytes on ultra-thin patterned parylene-C/silicon dioxide substrates. Biomaterials. 2011;32:2566-74.

[38] Unsworth CP, Graham ES, Delivopoulos E, Dragunow M, Murray AF. First human hNT neurons patterned on parylene-C/silicon dioxide substrates: Combining an accessible cell line and robust patterning technology for the study of the pathological adult human brain. J Neurosci Methods. 2010;194:154-7.

[39] Unsworth CP, Holloway H, Delivopoulos E, Murray AF, Simpson MC, Dickinson ME, et al. Patterning and detailed study of human hNT astrocytes on parylene-C/silicon dioxide substrates to the single cell level. Biomaterials. 2011;32:6541-50.

[40] Raos BJ, Unsworth CP, Costa JL, Rohde CA, Doyle CS, Bunting AS, et al. Infra-red laser ablative micromachining of parylene-C on SiO2 substrates for rapid prototyping, high yield, human neuronal cell patterning. Biofabrication. 2013;5:025006.

[41] Hughes MA, Bunting AS, Cameron K, Murray AF, Shipston MJ. Modulating patterned adhesion and repulsion of HEK 293 cells on microengineered parylene-C/SiO(2) substrates. J Biomed Mater Res A. 2013;101:349-57.

[42] Delivopoulos E, Ouberai MM, Coffey PD, Swann MJ, Shakesheff KM, Welland ME. Serum protein layers on parylene-C and silicon oxide: effect on cell adhesion. Colloids Surf B Biointerfaces. 2015;126:169-77.

[43] Trantidou T, Rao C, Barrett H, Camelliti P, Pinto K, Yacoub MH, et al. Selective hydrophilic modification of Parylene C films: a new approach to cell micro-patterning for synthetic biology applications. Biofabrication. 2014;6:025004.

[44] Golda-Cepa M, Engvall K, Kotarba A. Development of crystalline-amorphous parylene C structure in micro-and nano-range towards enhanced biocompatibility: the importance of oxygen plasma treatment time. Rsc Adv. 2015;5:48816-21.

[45] Unsworth CP, Delivopoulos E, Murray AF. Glimpsing Regular Lattice Arrangements of Primary Rat Hippocampal Astrocytes on Ultra-thin Nodes of Parylene-C. 18th Joint Symposium on Neural Computation2011.

[46] MacDonald C, Unsworth CP, Graham ES. Enrichment of differentiated hNT neurons and subsequent analysis using flow-cytometry and xCELLigence sensing. J Neurosci Methods. 2014;227:47-56.

[47] Hill EJ, Jimenez-Gonzalez C, Tarczyluk M, Nagel DA, Coleman MD, Parri HR. NT2 derived neuronal and astrocytic network signalling. PLoS One. 2012;7:e36098.

[48] Schneider CA, Rasband WS, Eliceiri KW. NIH Image to ImageJ: 25 years of image analysis. Nat Methods. 2012;9:671-5.